Science and Technology Indonesia
e-ISSN:2580-4391 *p*-ISSN:2580-4405
Vol. 10, No. 4, October 2025

Research Paper

Investigation of Mixed MeOH:EtOH Ratio and Air Supply on MEA Performance in Direct Alcohol Fuel Cell (DAFC)

Dwi Hawa Yulianti[1,2,4], Dedi Rohendi[2,3,4]*, Edy Herianto Majlan[5], Addy Rachmat[2,3,4], Nyimas Febrika Sya'baniah[1,2,4]

[1]*Chemistry Program, Faculty of Computer and Science, Universitas Indo Global Mandiri, Palembang, 30129, Indonesia*
[2]*Doctoral Program, Faculty of Mathematics and Natural Sciences, Universitas Sriwijaya, Palembang, 30139, Indonesia*
[3]*Department of Chemistry, Faculty of Mathematics and Natural Sciences, Universitas Sriwijaya, Ogan Ilir, 30662, Indonesia*
[4]*Center of Research Excellence in Fuel Cell and Hydrogen, Universitas Sriwijaya, Palembang, 30138, Indonesia*
[5]*Fuel Cell Institute, Universiti Kebangsaan Malaysia, Bangi, 43600, Malaysia*
***Corresponding author**: rohendi19@unsri.ac.id

Abstract
Methanol (MeOH) and ethanol (EtOH) are commonly used fuels in Direct Alcohol Fuel Cells (DAFC). The advantages of these two fuels are influenced by electrochemical reactions centered around the Membrane Electrode Assembly (MEA). In this study, Pt/C catalyst was used on the cathode and Pt-Ru/C on the anode, with catalyst loadings of 2, 4, 6, 8, and 10 mg/cm^2. The anode and cathode were characterized using Cyclic Voltammetry (CV), while the conductivity properties were evaluated through Electrochemical Impedance Spectroscopy (EIS). The Open Circuit Voltage (OCV) of the MEA in a single DAFC cell reached 0.65 V, with the highest value observed at a MeOH:EtOH volume ratio of 70:30 at concentrations of 3 M for MeOH and 2 M for EtOH. In addition to oxidation at the anode, oxygen reduction plays a significant role in the MEA performance on the cathode side. The oxygen supply to the cathode increased the power density by 52.17% at the optimal blower voltage of 5 V.

Keywords
DAFC, Pt-Ru/C, MeOH, EtOH, Blower

Received: 10 March 2025, Accepted: 3 July 2025
https://doi.org/10.26554/sti.2025.10.4.1012-1019

1. INTRODUCTION

Direct Alcohol Fuel Cells (DAFCs) have become a significant research focus due to their potential as on-demand energy sources, particularly for portable applications and electronic devices (Berretti et al., 2023). Low-molecular-weight alcohols, such as methanol (MeOH) and ethanol (EtOH), are considered among the most suitable fuels for DAFCs due to their simple molecular structure, high energy density (400-700 Wh/L), and low mass density, making them superior to hydrogen as a fuel for electrochemical cells (Bishnoi et al., 2024; Fadzillah et al., 2019). DAFCs generally use methanol (Direct Methanol Fuel Cell, DMFC) or ethanol (Direct Ethanol Fuel Cell, DEFC), each of which has specific characteristics with distinct advantages and limitations (Takahashi et al., 2024). Therefore, optimizing the fuel composition formulation is crucial to maximizing DAFC performance.

Although DAFCs have been implemented in everyday electronic devices such as laptops and mobile phones, their use still faces technical limitations (Fadzillah et al., 2019). Methanol exhibits high electrochemical reactivity, which enhances fuel cell performance; however, it is prone to crossover phenomena, where methanol directly migrates from the anode to the cathode, reducing system efficiency (Gagliardi et al., 2023; Zakaria et al., 2023). In contrast, ethanol has a lower crossover rate due to its larger molecular size and limited mobility, offering better operational stability (Bishnoi et al., 2024). The advantages and drawbacks of both fuels can be strategically leveraged to minimize crossover effects while enhancing energy conversion efficiency in DAFCs.

DAFC performance heavily depends on the efficiency of the Membrane Electrode Assembly (MEA), a critical component in electrochemical reactions, significantly influenced by the type of catalyst used (Jing et al., 2020). Platinum (Pt) is known as a superior catalyst due to its high corrosion resistance and effectiveness in improving electrochemical reaction kinetics. However, Pt is susceptible to carbon monoxide (CO) poisoning, which limits its performance. To mitigate this issue, it is often combined with other metals such as ruthenium (Ru) to reduce CO poisoning effects at the anode (Samad et al., 2018). The Pt-Ru combination has been proven effective in enhancing the long-term stability and efficiency of DAFCs. Previous

studies have demonstrated that variations in catalyst loading significantly affect MEA performance in passive DMFC systems. Building upon these findings, the present study extends the investigation to DAFC systems using methanol–ethanol blends to evaluate the effects of fuel composition and air supply on MEA performance more comprehensively (Yulianti et al., 2020).

On the other hand, Direct Ethanol Fuel Cells (DEFCs) offer a higher energy density (8 kWh/kg) compared to methanol (6.1 kWh/kg), making them superior in terms of energy storage capacity (Ahmed et al., 2022). Additionally, ethanol can be produced through biomass fermentation, which has the potential to reduce greenhouse gas emissions and promote energy sustainability. Thus, optimizing the methanol to ethanol mixing ratio is crucial for improving DAFC performance. The varying electrochemical characteristics of these two fuels enable the achievement of an optimal balance in specific compositions (Zhang et al., 2024). Previous studies have demonstrated that mixing methanol and ethanol in appropriate ratios can enhance fuel cell performance by leveraging the high electrochemical activity of methanol and the lower crossover tendency of ethanol, thereby improving overall efficiency and operational stability. An adequate oxygen supply to the cathode is crucial for enhancing the rate of the oxygen reduction reaction, reducing overpotential, and preventing heat accumulation (Chen et al., 2024; Kang et al., 2020). Furthermore, the performance of DAFC can be notably enhanced by regulating the air supply at the cathode through a blower mechanism, which not only facilitates faster electrochemical reaction kinetics and improves overall energy conversion efficiency, but also enhances oxygen transport through forced convection, leading to higher current and power densities and thereby supporting stable and sustainable operation (Berretti et al., 2023).

This study aligns with Sustainable Development Goal (SDG) 7, which promotes affordable and clean energy by advancing the development of efficient and environmentally sustainable alternative energy technologies. Using methanol and ethanol as fuel sources in Direct Alcohol Fuel Cells (DAFC) can reduce dependence on fossil fuels and consequently lower CO_2 emissions, thereby contributing to global climate change mitigation efforts (Che Ramli et al., 2024). This study aims to investigate the effect of methanol–ethanol fuel composition and cathode air supply on the performance of DAFCs. The focus is on optimizing fuel formulation and operating conditions to enhance energy conversion efficiency and long-term stability, thereby supporting the development of sustainable and high-performance energy systems.

2. EXPERIMENTAL SECTION

2.1 Materials

Carbon paper Avcarb P75T (Fuel Cell store), carbon Vulcan XC-72R (FuelCell store), Polytetrafluoroethylene (PTFE) Dispersion TE 3869 60 wt% (FuelCell store), membrane Nafion-117 (FuelCell store), Nafion solution DE 1021 10 wt% (FuelCell store), 2-propanol (Mercks), Pt/C and Pt-Ru/C (40%) (FuelCell store), NaOH (Mercks), H_2O_2 (Mercks) and H_2SO_4 (Mercks).

2.2 Methods

The electrode was fabricated by spraying a catalyst layer ink onto the Gas Diffusion Layer (GDL). The catalyst layer was prepared by mixing Pt-Ru/C catalyst powder (Fuel Cell Store) for the anode side and Pt/C for the cathode side, with varying catalyst loadings of 2, 4, 6, 8, and 10 mg/cm^2. 2-propanol, Nafion DE 1021 10 wt% solution, and PTFE Dispersion TE 3869 60 wt% were added to the mixture and stirred using an ultrasonic homogenizer to produce a catalyst ink. This ink was then sprayed onto the GDL surface using a spray gun. The GDL consists of a carbon paper support layer and a microporous layer containing Vulcan (XC-72R), PTFE, and isopropyl alcohol. The GDL was sintered at 350°C for 3 hours to enhance PTFE absorption into the carbon paper pores, enhancing its hydrophobic properties.

The fabricated electrodes were characterized using X-ray diffraction (XRD) with a Rigaku MiniFlex 600. Electrochemical characterization was performed using cyclic voltammetry (CV) to determine the Electrochemical Surface Area (ECSA) and Electrochemical Impedance Spectroscopy (EIS) to assess electrical conductivity, with a scan rate of 25 mV/s using a Potentiostat/Galvanostat Autolab PGSTAT204 from Metrohm. The measurement setup consisted of a three-electrode system: a working electrode (Pt-Ru/C), a counter electrode (Pt), and a reference electrode (Ag/AgCl), with 1 M NaOH as the electrolyte.

The anode and cathode, each with a surface area of 16 cm^2, were placed on either side of a Nafion-117 membrane and assembled through hydraulic lamination using a hot press (EQ-HP-88V-LD) at 135°C for 3 minutes under a pressure of 2000 psi to produce MEA . An illustration of the MEA fabrication process is given in Figure 1.

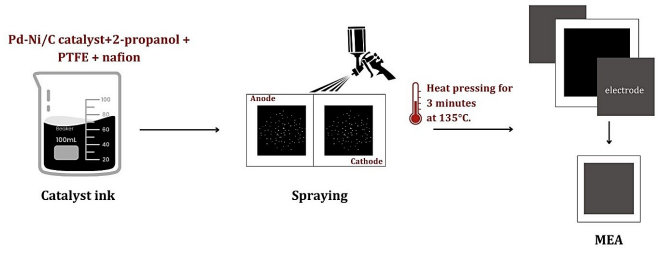

Figure 1. Illustration of MEA Fabrication Using the Spraying Method

3. RESULTS AND DISCUSSION

3.1 Characterization of Electrodes

3.1.1 XRD Analysis

Electrode characterization was conducted using XRD, CV, and EIS analyses. XRD analysis was used to identify the crystal

structure of the material. As shown in the diffractogram in Figure 2, sharp peaks were observed in the 20°–30° region, indicating the presence of carbon atoms (JCPDS No. 50-926) (Dehghani Sanij and Gharibi, 2018). Peaks below 20° correspond to the presence of PTFE and Nafion (Li et al., 2023).

For the Pt/C electrode, platinum peaks were detected at 39.7° (JCPDS 04-0802) (Yulianti et al., 2020), whereas for the Pt-Ru/C electrode, platinum was identified at 40.47°. In the Pt-Ru/C catalyst, Ru was predominantly present in an alloy form with Pt, as the diffraction peaks of pure Ru were observed with low crystal intensity and an amorphous structure. The incorporation of Ru atoms into Pt contributes to its catalytic properties (Wang et al., 2021). Additionally, Ru atoms were detected at approximately 58.3°, indicating the presence of Ru in a crystalline phase, although with relatively low intensity due to the predominant alloy formation with Pt (Liu et al., 2020).

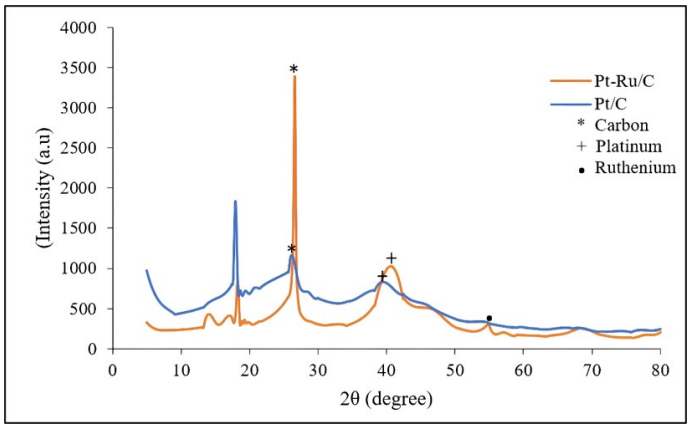

Figure 2. X-Ray Diffractogram of Electrodes with Pt/C and Pt-Ru/C Catalysts

Based on measurements using the Debye-Scherrer equation, the crystallite size of platinum in the Pt/C electrode was found to be 0.596 nm, while the crystallite size of ruthenium in the Pt-Ru/C electrode was 6.871 nm. These results indicate a significant difference in size, with ruthenium forming larger crystallites than platinum. This size variation can influence the distribution of active surface areas and the interaction between catalyst particles, affecting the electrocatalytic activity and stability of the electrode in fuel cells.

3.1.2 Electrochemical Analysis

The electrocatalytic activity of each electrode can be determined using the CV method. This analysis is performed to measure and analyze the electrochemical activity of the catalyst through the calculation of the ECSA. Characterization was conducted within a potential range of -0.2 V to 0.4 V with a scan rate of 25 mV/s (Yahya et al., 2019). The voltage range in CV depends on the type of reaction and the electrochemical reaction area represented by the current peaks. CV measurements show an anodic peak and a cathodic peak. The anodic peak indicates the oxidation capability, while the cathodic peak shows the reduction capability of the catalyst on the electrode. The higher the current and potential values attained, the greater the electrode's oxidation capability. The appearance of peaks in CV measurements is attributed to chemisorption on the catalyst surface and mass transport processes.

The voltammogram from the electrode characterization with the Pt-Ru/C catalyst shows that, based on the ECSA calculation, the electrode with a catalyst loading of 10 mg/cm^2 has the highest ECSA value, which is 3,984.76 cm^2/g. This electrochemical surface area can be calculated using Equation (1).

$$ECSA = \frac{Q}{\Gamma.L} \quad (1)$$

with Q as the integrated charge density (C/cm^2), Γ as the specific charge required to oxidize or reduce a monolayer of adsorbed species (μC/cm^2), and L as the platinum loading on the electrode (mg/cm^2). According to Equation (1), the higher the catalyst loading, the higher the ECSA value obtained, which aligns with previous research (Yulianti et al., 2020). However, this also depends on the amount of electric charge, which indicates the catalytic activity of the (Martínez-Hincapié et al., 2024). The curve illustrating the relationship between catalyst loading and ECSA value is presented in Figure 3.

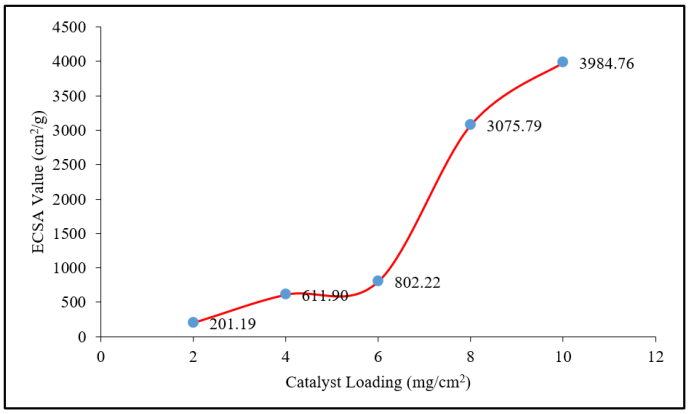

Figure 3. Effect of Catalyst Loading on ECSA Value

The electrical conductivity of the electrode was determined using the EIS methods. This conductivity analysis provides insights into the electrode's ability to conduct the flowing electrical current. The electrical conductivity of the electrode was determined through the fitting of the Nyquist curve according to Equation (2) (Gandomi et al., 2020).

$$\sigma = \frac{1}{Z_R} \times \frac{l}{A} \quad (2)$$

where σ is the electrical conductivity (S/cm); ZR is the real impedance (Ω) = Rp + Rs; l is the length/thickness of the electrode (cm); and A is the electrode surface area (cm^2) (Rohendi et al., 2024).

Based on the calculation of electrical conductivity, the highest value was obtained for the Pt-Ru/C electrode with a catalyst loading of 10 mg/cm^2, as presented in Figure 4. This finding highlights the catalyst's ability in the electrode to interact electrochemically and facilitate the flow of electrical energy. Additionally, the role of the catalyst in generating electrical energy is influenced by the number of active sites (ECSA) available. These active sites are the primary locations where electrochemical processes occur, reflecting the electrode's capability to convert energy efficiently (Rohendi et al., 2023). As shown in Figure 4, the electrical conductivity values vary with different catalyst loadings. While the highest conductivity of 108.45 S/cm was achieved at 10 mg/cm^2, the lowest conductivity of 55.28 S/cm^2 was observed at 4 mg/cm^2. This suggests that an optimal catalyst loading is crucial for maximizing conductivity, as insufficient or excessive catalyst amounts may affect the uniformity of catalyst distribution and electron transfer efficiency within the electrode structure (Kreider et al., 2024).

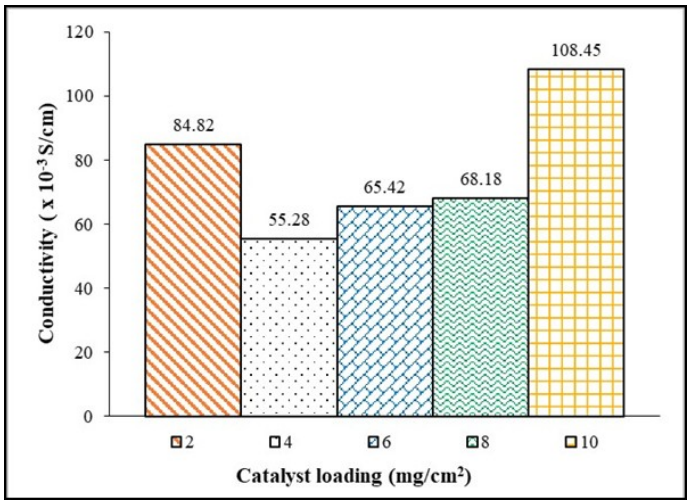

Figure 4. Effect of Catalyst Loading on Electrode Conductivity

However, at a catalyst loading of 4 mg/cm^2, the electrical conductivity was the lowest among all variations, recorded at 55.28 S/cm. This could be attributed to several factors. First, an uneven distribution of the catalyst at this loading might result in certain areas of the electrode having a lower density of active sites, thereby hindering electron transfer. Second, an imbalance between conductivity and reactivity may occur, where at this particular catalyst loading, the interaction between catalyst particles within the electrode network is less optimal, reducing the effectiveness of conductivity pathways. Third, the presence of higher internal resistance in the electrode could be a contributing factor, as the amount of catalyst may not be sufficient to form efficient electron pathways. Thus, the lower conductivity observed at the catalyst loading of 4 mg/cm^2, compared to 2 mg/cm^2 and 6 mg/cm^2, could be due to an uneven distribution of catalyst, suboptimal conductive pathways, or increased internal resistance within the electrode structure (Pan et al., 2024).

3.2 MEA Performance with Varying Catalyst Loading

The electrochemical process generally occurs at the catalyst layer, where the more active sites the catalyst has the more optimal the reaction. This process is influenced by the catalyst loading. As the catalyst loading increases, the performance of the MEA is expected to improve. However, the catalyst's performance on the electrode also depends on the distribution of the catalyst itself (Kim et al., 2021). The MEA performance with varying catalyst loading using a 3 M methanol and 2 M ethanol fuel mixture at a 50:50 volume ratio is shown in Figure 5.

Based on Figure 5, it can be observed that as the catalyst loading increases, the MEA performance also improves. The MEA with a catalyst loading of 2 mg/cm^2 shows the lowest performance. The number of active sites on the catalyst is directly related to the amount of catalyst distributed on the GDL surface. The MEA with a catalyst loading of 10 mg/cm^2 exhibits the best performance, particularly in the activation polarization and ohmic polarization regions, as it maintains voltage stability with increasing current.

Ohmic polarization occurs due to significant interfacial resistance, resulting in increased resistance at the electrode and hindering proton transport (Wallnöfer-Ogris et al., 2024), which is shown by a voltage decrease. At a current density of 8 mA/cm^2, a voltage drop occurs, indicating the presence of concentration polarization. This concentration polarization is caused by fuel evaporation, which leads to a reduction in fuel concentration, ultimately decreasing the MEA's ability to maintain voltage and handle the applied load.

3.3 MEA Performance with Varying MeOH:EtOH Volume Ratio

The initial performance of the MEA in the DAFC is evaluated without load, known as Open Circuit Voltage (OCV). OCV represents the operational condition of the fuel cell when no external load or current is applied, meaning the circuit is open, allowing the fuel cell to maintain the maximum potential difference between the anode and cathode, and it reflects the minimum electrical power required per unit of current in a reaction (Cammarata and Mastropasqua, 2023). OCV reflects the electrochemical potential inherent in the fuel cell and provides information regarding the theoretical maximum efficiency without any external load. The OCV results for the DAFC with different methanol to ethanol ratios offer a comparative understanding of how various fuel mixtures affect the base performance of the cell. These results are summarized in Table 1, highlighting the effects of different methanol to ethanol ratios on OCV, which can further be correlated with the catalytic efficiency of the fuel cell, fuel utilization, and the potential reaction kinetics.

Based on Table 1, it can be analyzed that at a MeOH:EtOH composition of 10:90, a small in OCV is observed. This is due to strong competitive adsorption between methanol and

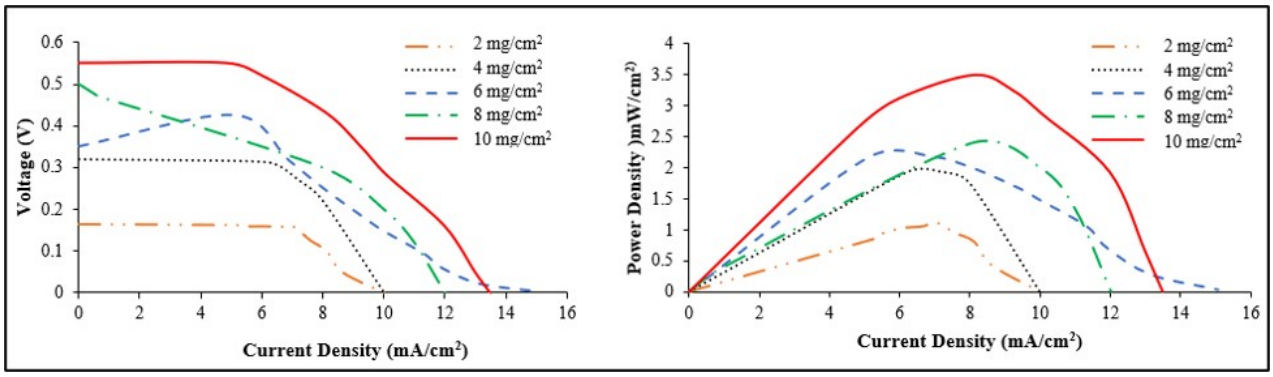

Figure 5. Performance Curves of MEA with Varying Catalyst Composition (a) I-V and (b) I-P Performance

ethanol on the catalyst surface. However, as the methanol composition increases, the OCV value rises and stabilizes, eventually reaching an optimum point at a MeOH:EtOH ratio of 70:30, with an OCV value of 0.65 V. Methanol has good mobility, but at higher concentrations, it can cause crossover, which leads to a decrease in MEA performance. Crossover occurs when methanol migrates from the anode side to the cathode side without undergoing the splitting process, and an increase in temperature may cause damage to the MEA (Rashidi et al., 2022).

Table 1. OCV Values with Varying MeOH:EtOH Ratios

MeOH:EtOH	OCV value (V)
10:90	0.390
20:80	0.439
30:70	0.480
40:60	0.513
50:50	0.555
60:40	0.594
70:30	0.650
80:20	0.543
90:10	0.440

3.4 The Operation Time of DAFC

The operation time of DAFC with a single fuel charge was evaluated using a MeOH:EtOH composition of 70:30, which was chosen due to its good electrochemical properties. This test involved the continuous operation of the DAFC over a long period to observe the ability of the MEA to maintain voltage during use (Xie et al., 2021). As shown in Figure 6, the durability of MEA in DAFC is characterized by minimal voltage degradation over time, reflecting stable electrochemical properties and structural integrity of MEA with a decrease in concentration and volume of fuel. Additionally, the 70:30 MeOH ratio helps reduce unwanted oxidation reactions, contributing to sustained performance in long-term use. This demonstrates the suitability of the MEA for applications requiring reliable and durable DAFC performance. The DAFC performance with a catalyst loading of 10 mg/cm^2 at a MeOH:EtOH fuel composition of 70:30 with a single fuel charge (±13 mL) is presented in Figure 6.

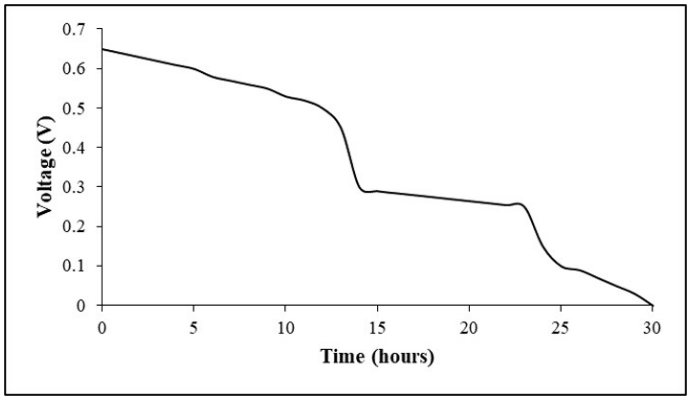

Figure 6. DAFC Performance with a Catalyst Loading of 10 mg/cm^2 at MeOH:EtOH = 70:30

The DAFC performance was measured at a constant current of 0.1 A. Voltage degradation occurred with increased operating time and decreased fuel concentration. The voltage decreased by approximately 23% from the start of the test until 12 hours of operation, then dropped to around 3 V during the 13-23 hours period and gradually declined until the voltage could no longer be maintained at 30 hours of operation. This indicates that the MEA performance declined due to the decreasing fuel concentration (Sung et al., 2025). The consequence of this condition is a decline in MEA performance (Hu et al., 2021). Another factor that could contribute to the reduced MEA performance over long-term use is structural changes in the catalyst, which lead to agglomeration and a reduction in the catalyst's active sites.

3.5 MEA Performance with Varying Blower Voltage

The addition of a blower at the cathode as an oxygen supply source can enhance the electrical power output of the MEA (Gupta and Pramanik, 2019). Performance testing was con-

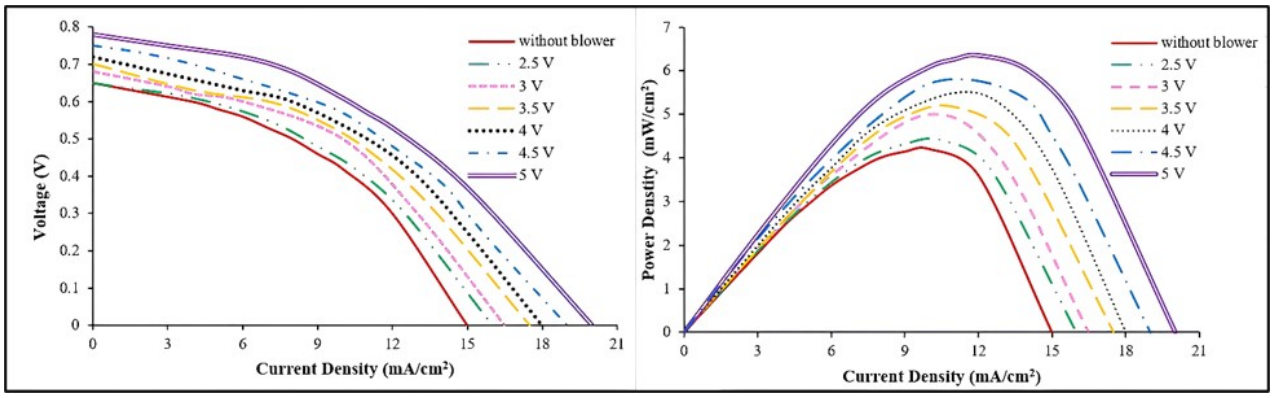

Figure 7. MEA Performance with Varying Blower Voltage

ducted with a catalyst loading of 10 mg/cm^2 and a fuel mixture of 3 M methanol and 2 M ethanol in a 70:30 ratio. The amount of oxygen at the cathode (supplied by increasing the air supply through the blower) is crucial to the reaction results. The oxygen supply must match the required amount for maximum power output, which is regulated by adjusting the blower voltage. The performance of the MEA with varying airflow rates is shown in Figure 7.

Based on the performance measurements with the addition of air to supply oxygen to the cathode, there was an observed effect on MEA performance. The best performance was achieved with the blower operating at 5 V. This improved performance by 52.17% compared to the case without using the blower. The oxygen supply to the cathode affects MEA performance and can also serve as a cooling stack, reducing heat generated during crossover (Chen et al., 2024; Kang et al., 2020).

4. CONCLUSIONS

The optimal performance of the Membrane Electrode Assembly (MEA) in Direct Alcohol Fuel Cells (DAFC) was achieved using a Pt-Ru/C anode catalyst and a MeOH:EtOH fuel composition ratio of 70:30. The presence of ethanol in the fuel mixture acts as an effective balancing agent due to its larger molecular size and lower mobility, which helps suppress the methanol crossover rate. This crossover rate typically increases with higher methanol concentrations, as a greater concentration gradient drives methanol diffusion from the anode to the cathode, potentially reducing the long-term efficiency and stability of the MEA. Furthermore, regulating the oxygen supply at the cathode using a blower has been shown to significantly enhance the oxygen reduction reaction and overall energy conversion efficiency, thereby supporting more stable and efficient DAFC performance.

5. ACKNOWLEDGMENT

Acknowledgement The author expresses gratitude and appreciation to Universitas Indo Global Mandiri (UIGM) for funding this research and to Universitas Sriwijaya for providing the research facilities through the Center of Research Excellence in Fuel Cell and Hydrogen, Universitas Sriwijaya.

REFERENCES

Ahmed, A. A., M. Al Labadidi, A. T. Hamada, and M. F. Orhan (2022). Design and Utilization of a Direct Methanol Fuel Cell. *Membranes*, **12**(12); 1–22

Berretti, E., L. Osmieri, V. Baglio, H. A. Miller, J. Filippi, F. Vizza, M. Santamaria, S. Specchia, C. Santoro, and A. Lavacchi (2023). Direct Alcohol Fuel Cells: A Comparative Review of Acidic and Alkaline Systems. *Electrochemical Energy Reviews*, **6**(1); 1–50

Bishnoi, P., K. Mishra, S. S. Siwal, V. K. Gupta, and V. K. Thakur (2024). Direct Ethanol Fuel Cell for Clean Electric Energy: Unravelling the Role of Electrode Materials for a Sustainable Future. *Advanced Energy and Sustainability Research*, **5**(6); 1–37

Cammarata, A. and L. Mastropasqua (2023). Theoretical Analysis of Mixed Open-Circuit Potential for High Temperature Electrochemical Cells Electrodes. *Frontiers in Energy Research*, **11**; 1–8

Che Ramli, Z. A., J. Pasupuleti, A. M. Zainoodin, N. F. H. Nik Zaiman, K. N. Ahmad, N. F. Raduwan, Y. N. Yusoff, W. N. R. Wan Isahak, T. S. Tengku Saharuddin, and S. T. Kiong (2024). Unlocking the Potential of Pt-Based and Metal Oxides Catalysts in Liquid Fuel Cells Technologies: Performance and Challenges. *Ain Shams Engineering Journal*, **15**(12); 1–31

Chen, J., L. Sun, W. Zhu, H. Pei, L. Xing, and Z. Tu (2024). Influence of Cathode Air Supply Mode on the Performance of an Open Cathode Air-Cooled Proton Exchange Membrane Fuel Cell Stack. *Applied Thermal Engineering*, **243**; 1–9

Dehghani Sanij, F. and H. Gharibi (2018). Preparation of Bimetallic Alloyed Palladium-Nickel Electro-Catalysts Supported on Carbon with Superior Catalytic Performance Towards Oxygen Reduction Reaction. *Colloids and Surfaces A: Physicochemical and Engineering Aspects*, **538**; 429–442

Fadzillah, D. M., S. K. Kamarudin, M. A. Zainoodin, and

M. S. Masdar (2019). Critical Challenges in the System Development of Direct Alcohol Fuel Cells as Portable Power Supplies: An Overview. *International Journal of Hydrogen Energy*, **44**(5); 3031–3054

Gagliardi, G. G., A. El-Kharouf, and D. Borello (2023). Assessment of Innovative Graphene Oxide Composite Membranes for the Improvement of Direct Methanol Fuel Cells Performance. *Fuel*, **345**; 1–10

Gandomi, Y. A., D. S. Aaron, Z. B. Nolan, A. Ahmadi, and M. M. Mench (2020). Direct Measurement of Crossover and Interfacial Resistance of Ion-Exchange Membranes in All-Vanadium Redox Flow Batteries. *Membranes*, **10**(6); 1–21

Gupta, U. K. and H. Pramanik (2019). Electrooxidation Study of Pure Ethanol/Methanol and Their Mixture for the Application in Direct Alcohol Alkaline Fuel Cells (DAAFCs). *International Journal of Hydrogen Energy*, **44**(1); 421–435

Hu, Z., L. Xu, Q. Gan, X. Du, W. Dai, Q. Wang, W. Zheng, Y. Ding, J. Li, and M. Ouyang (2021). Carbon Corrosion Induced Fuel Cell Accelerated Degradation Warning: From Mechanism to Diagnosis. *Electrochimica Acta*, **389**; 1–10

Jing, F., R. Sun, S. Wang, H. Sun, and G. Sun (2020). Effect of the Anode Structure on the Stability of a Direct Methanol Fuel Cell. *Energy and Fuels*, **34**(3); 3850–3857

Kang, D. G., C. Park, I. S. Lim, S. H. Choi, D. K. Lee, and M. S. Kim (2020). Performance Enhancement of Air-Cooled Open Cathode Polymer Electrolyte Membrane Fuel Cell with Inserting Metal Foam in the Cathode Side. *International Journal of Hydrogen Energy*, **45**(51); 27622–27631

Kim, S., M. Her, Y. Kim, C. Y. Ahn, S. Park, Y. H. Cho, and Y. E. Sung (2021). The Impact of the Catalyst Layer Structure on the Performance of Anion Exchange Membrane Fuel Cell. *Electrochimica Acta*, **400**; 1–10

Kreider, M. E., H. Yu, L. Osmieri, M. R. Parimuha, K. S. Reeves, D. H. Marin, R. T. Hannagan, E. K. Volk, T. F. Jaramillo, J. L. Young, P. Zelenay, and S. M. Alia (2024). Understanding the Effects of Anode Catalyst Conductivity and Loading on Catalyst Layer Utilization and Performance for Anion Exchange Membrane Water Electrolysis. *ACS Catalysis*, **14**(14); 10806–10819

Li, Z., X. Qi, C. Liu, B. Fan, and X. Yang (2023). Particle Size Effect of PTFE on Friction and Wear Properties of Glass Fiber Reinforced Epoxy Resin Composites. *Wear*, **532–533**; 1–12

Liu, X., G. Jiang, Y. Tan, S. Luo, M. Xu, Y. Jia, P. Lu, and Y. He (2020). Highly-Dispersed Ruthenium Precursors: Via a Self-Assembly-Assisted Synthesis of Uniform Ruthenium Nanoparticles for Superior Hydrogen Evolution Reaction. *RSC Advances*, **10**(24); 14313–14316

Martínez-Hincapié, R., J. Wegner, M. U. Anwar, A. Raza-Khan, S. Franzka, S. Kleszczynski, and V. Čolić (2024). The Determination of the Electrochemically Active Surface Area and Its Effects on the Electrocatalytic Properties of Structured Nickel Electrodes Produced by Additive Manufacturing. *Electrochimica Acta*, **476**; 1–10

Pan, Y., H. Liu, J. Liu, L. Wen, K. Lao, S. Li, X. Fang, H. Wang, H. B. Tao, and N. Zheng (2024). Probing Current Density Distribution Over a Catalyst Layer at the Micrometer Scale in a Water Electrolyzer. *Catalysis Science and Technology*, **14**(6); 1480–1487

Rashidi, S., N. Karimi, B. Sunden, K. C. Kim, A. G. Olabi, and O. Mahian (2022). Progress and Challenges on the Thermal Management of Electrochemical Energy Conversion and Storage Technologies: Fuel Cells, Electrolysers, and Supercapacitors. *Progress in Energy and Combustion Science*, **88**; 1–50

Rohendi, D., E. H. Majlan, D. H. Yulianti, Juwita, N. Syarif, A. Rachmat, A. Sumboja, F. S. Nyimas, and I. Amelia (2024). Performance of Membrane Electrode Assembly Using Pt/C and CoFe/N-C Catalysts in Proton Exchange Membrane Fuel Cells. *Malaysian Journal of Analytical Sciences*, **28**(2); 388–396

Rohendi, D., N. F. Sya'baniah, E. H. Majlan, N. Syarif, A. Rachmat, D. H. Yulianti, I. Amelia, D. Ardiyanta, I. Mahendra, and R. W. H. Erliana (2023). The Electrochemical Conversion of CO2 into Methanol with KHCO3 Electrolyte Using Membrane Electrode Assembly (MEA). *Science and Technology Indonesia*, **8**(4); 632–639

Samad, S., K. S. Loh, W. Y. Wong, T. K. Lee, J. Sunarso, S. T. Chong, and W. R. Wan Daud (2018). Carbon and Non-Carbon Support Materials for Platinum-Based Catalysts in Fuel Cells. *International Journal of Hydrogen Energy*, **43**(16); 7823–7854

Sung, M., H. Yi, J. Han, J. B. Lee, and S. Yoon (2025). Carbon Nanofiber-Reinforced Carbon Black Support for Enhancing the Durability of Catalysts Used in Proton Exchange Membrane Fuel Cells Against Carbon Corrosion. *Membranes*, **15**(3); 1–16

Takahashi, Y., H. Semizo, and Y. Matsuo (2024). Power Generation Characteristics and Optimum Alcohol Concentration in Bio-Direct Alcohol Fuel Cell Using Chitin Family Electrolyte. *Chemical Physics Impact*, **8**; 1–8

Wallnöfer-Ogris, E., I. Grimmer, M. Ranz, M. Höglinger, S. Kartusch, J. Rauh, M. G. Macherhammer, B. Grabner, and A. Trattner (2024). A Review on Understanding and Identifying Degradation Mechanisms in PEM Water Electrolysis Cells: Insights for Stack Application, Development, and Research. *International Journal of Hydrogen Energy*, **65**; 381–397

Wang, Q., Y. W. Zhou, Z. Jin, C. Chen, H. Li, and W. B. Cai (2021). Alternative Aqueous Phase Synthesis of a PtRu/C Electrocatalyst for Direct Methanol Fuel Cells. *Catalysts*, **11**(8); 1–14

Xie, Z., L. Tian, W. Zhang, Q. Ma, L. Xing, Q. Xu, L. Khotseng, and H. Su (2021). Enhanced Low-Humidity Performance of Proton Exchange Membrane Fuel Cell by Incorporating Phosphoric Acid-Loaded Covalent Organic Framework in Anode Catalyst Layer. *International Journal of Hydrogen Energy*, **46**(18); 10903–10912

Yahya, N., S. K. Kamarudin, N. A. Karim, M. S. Masdar, K. S.

Loh, and K. L. Lim (2019). Durability and Performance of Direct Glycerol Fuel Cell with Palladium-Aurum/Vapor Grown Carbon Nanofiber Support. *Energy Conversion and Management*, **188**; 120–130

Yulianti, D. H., D. Rohendi, N. Syarif, and A. Rachmat (2020). Characterization of Electrode with Various of Pt-Ru/C Catalyst Loading and the Performance Test of Membrane Electrode Assembly (MEA) in Passive Direct Methanol Fuel Cell (DMFC). *Key Engineering Materials*, **840**; 558–565

Zakaria, Z., S. K. Kamarudin, and K. A. A. Wahid (2023). Polymer Electrolyte Membrane Modification in Direct Ethanol Fuel Cells: An Update. *Journal of Applied Polymer Science*, **140**(4); 1–20

Zhang, X., Z. Yang, and J. Chen (2024). Performance Analysis and Optimum Design of a Direct Alcohol Fuel Cell Fueled With Mixed Alcohols. *Journal of Energy Resources Technology, Part A: Sustainable and Renewable Energy*, **1**(1); 1–11